Acta Crystallographica Section D
Biological Crystallography
ISSN 0907-4449

Crystallographic analysis of the dsDNA bacteriophage HK97 mature empty capsid

William R. Wikoff,[a,b] Robert L. Duda,[c] Roger W. Hendrix[c] and John E. Johnson[a]*

[a]Department of Molecular Biology, The Scripps Research Institute, 10550 North Torrey Pines Road, La Jolla, CA 92037, USA, [b] Department of Biological Sciences, Purdue University, West Lafayette, IN 47907, USA, and [c]Department of Biological Sciences, University of Pittsburgh, Pittsburgh, PA 15260, USA

Correspondence e-mail: jackj@scripps.edu

Received 30 January 1998
Accepted 15 December 1998

HK97 is a member of the *Siphovirus* family of dsDNA bacteriophages. It is similar in architecture to bacteriophage λ, the type member of this family, with an icosahedral capsid of triangulation number $T = 7$. No high-resolution structural information is available for the dsDNA phages, and HK97 is the only dsDNA bacteriophage capsid to produce crystals which diffract X-rays. At 650 Å in diameter, the large size of the particle and resultant large unit cell create crystallographic challenges. The empty Head II (mature) particles were expressed in *Escherichia coli* and assembled *in vitro*, but they have the same morphology as the mature HK97 capsid. Previously reported Head II crystals diffracting to 3.5 Å resolution are examined here in detail. Although the cell dimensions suggest an orthorhombic lattice, further analysis demonstrated that the space group was monoclinic. This has been confirmed by the present study. Images were recorded on the F1 beamline at CHESS and they were processed and scaled, resulting in a data set with a cumulative completeness of 65% and a scaling R factor of 7.7% to 7 Å. The cell dimensions after post-refinement were $a = 580$, $b = 626$, $c = 788$ Å, $\beta = 90.0^\circ$. From the particle dimensions determined by cryo-electron microscopy (cryo-EM), there were determined to be two particles per unit cell. Systematic absences of even reflections along the $0k0$ lattice line indicate that the space group is $P2_1$. The rotation function was used to determine the orientation of the particles in the unit cell and to confirm the space group. An icosahedral twofold axis is approximately, but not exactly, aligned with the crystallographic screw (b) axis. An icosahedral twofold axis orthogonal to the one approximately parallel to the b axis, is rotated 18° away from the a axis. The centers of the two particles must be positioned close to the minimum-energy packing arrangement for spheres, which places one particle at $(\frac{1}{4}, 0, \frac{1}{4})$ and the other particle at $(\frac{3}{4}, \frac{1}{2}, \frac{3}{4})$. The particle position and orientation were confirmed by calculating a Patterson function. The particles interact closely along icosahedral threefold axes, which occurs both along the crystallographic a axis and along the b axis. The particle dimensions derived from this packing arrangement agree well with those determined by cryo-EM and image reconstruction. The cryo-EM reconstruction will be used as a model to initiate phase determination; structure determination at 7 Å is under way.

1. Introduction

Bacteriophages are one of the primary structural, biochemical and molecular-biological model systems in modern biology. The dsDNA bacteriophages infect a wide variety of bacterial hosts and occupy diverse environments, including aquatic, soil

and animal systems. A phage particle is constructed from many copies of one or more gene products arranged with icosahedral symmetry. The capsid contains the DNA genome and has a tail assembly through which the DNA is injected after the particle attaches to the cell. The assembly of a phage particle into this architecturally complex structure has been extensively studied; several phage-assembly pathways have been characterized in detail (Casjens & Hendrix, 1988). All well studied dsDNA bacteriophage groups share several common features of structure and assembly. These include the $T = 7$ quasi-equivalent arrangement of capsid subunits (in phages with known structure), the assembly of empty capsids into provirions, the packaging of dsDNA through a 'portal complex' at a unique pentamer and the expansion and extensive conformational change that occurs when the dsDNA is packaged into the provirion; the resultant particle has increased stability. This elaborate, highly regulated assembly and maturation pathway has been thoroughly investigated. The assembly and genome organization of dsDNA phages is more complex than that of the small spherical plant and animal viruses.

The most detailed structural information on dsDNA bacteriophage capsids has been determined by cryo-electron microscopy and image reconstruction (Conway *et al.*, 1995; Dokland *et al.*, 1992; Dokland & Murialdo, 1993; Prasad *et al.*, 1993). Bacteriophage structure has also been investigated by X-ray solution scattering (King *et al.*, 1976; Stroud *et al.*, 1981) and spectroscopy (Li *et al.*, 1981; Prevelige *et al.*, 1993; Steven *et al.*, 1990; Thomas *et al.*, 1982). Despite previous attempts, no high-resolution structures have been determined, primarily because crystals which diffracted X-rays could not be grown. The bacteriophage capsids are relatively large and are close to the current size limit of macromolecules accessible to X-ray crystallography.

A medium- or high-resolution structure of a dsDNA bacteriophage will provide information about the capsid architecture of the protein subunit and of the quaternary interactions between subunits, and thus information about capsid assembly. Most of the small plant and animal viruses for which high-resolution structures are known have subunit folds built around a characteristic β-barrel. The dsDNA phages may reveal a novel capsid protein architecture.

An understanding of the assembly process for bacteriophages should provide insight into the analogous process which occurs in some animal viruses. For example, herpesviruses share a number of features in common with dsDNA bacteriophages. Like most phages, herpesviruses assemble an empty procapsid with a scaffold. A protease is then activated and cleaves two internal proteins, and the shell transforms in a conformational change analagous to the bacteriophage-expansion reaction that occurs upon dsDNA packaging (Newcomb *et al.*, 1996; Trus *et al.*, 1996). None of the virus capsid proteins with known structures exhibit a conformational change during assembly analogous to the expansion reaction seen in the dsDNA bacteriophages and in herpesvirus. The *Papovaviridae*, with a capsid organization which is reminiscent of the $T = 7$ quasi-equivalent organization found in bacteriophages, is the only dsDNA virus group for which an X-ray structure is known (Liddington *et al.*, 1991). The capsid arrangement deviates from the classic $T = 7$ symmetry by placing pentamers in the position which would ordinarily be occupied by hexamers. The other large dsDNA viruses, including herpesvirus, hepatitis virus and adenovirus, have not been accessible to X-ray crystallography, although the capsid subunit of adenovirus has been studied at high resolution as an oligomer called the hexon (Roberts *et al.*, 1986). Thus, an understanding of how quasi-equivalence is utilized in phages and the structural details of the assembly process may add to the understanding of animal virus structure and assembly.

The dsDNA bacteriophage HK97 belongs to the *Siphovirus* group (Murphy *et al.*, 1995); the type-member of this group is phage λ. The assembly of the HK97 capsid has been characterized in detail and is an excellent system for the study of virus assembly. During the maturation process, the capsid goes through three intermediate forms before it reaches the final Head II capsid state (Conway *et al.*, 1995). By expressing the capsid protein and the putative protease in the native and mutant forms, it is possible to produce each of the four particle types; for each of these, a cryo-EM reconstruction has been determined (Conway *et al.*, 1995). Assembly begins when 420 copies of the uncleaved capsid protein (gp5) are arranged in pentamers and hexamers into a $T = 7$ icosahedron, termed Prohead I. Approximately 50 copies of gp4, the putative protease, are packaged inside the capsid. Prohead II is formed after 102 amino-acid residues are cleaved from the amino-terminus of each gp5 molecule; the protease and these proteolytically cleaved fragments then leave the capsid. The prohead-to-head transition (Prohead II to Head II) occurs *in vivo* when dsDNA is packaged into the capsid; the equivalent structural changes can be induced *in vitro* in various partially denaturing solvent conditions. The final maturation step to the Head II particle is a covalent crosslinking reaction which joins a lysine to an asparagine residue with an amide bond, linking the entire capsid into concatenated circles and providing stability to the capsid.

This paper describes the second phase of the crystallographic investigation of empty Head II capsid crystals, including space-group determination, data analysis and determination of the particle orientation, position and packing. At 650 Å in diameter along the fivefold axis, these are among the largest virus particles to be studied by X-ray crystallography to date. This is the first example of a dsDNA bacteriophage to yield high-resolution structural data.

2. Materials and methods

The production, purification and crystallization of the empty Head II particle crystals was were previously described (Wikoff *et al.*, 1998). Briefly, HK97 empty capsids were produced in *Escherichia coli* by expressing the gp4 (putative protease) and gp5 (capsid protein). These 'immature' capsids were purified and expanded *in vitro* to produce the mature empty capsid (Head II). Crystals were grown directly in the X-ray capillary by mixing an equal volume (4 ml) of virus at

40–70 mg ml^{-1} and precipitant. The precipitant mix consisted of 50 m*M* citrate pH 5.0, 0.85 *M* ammonium sulfate and 1.5% PEG 8000. Data to about 5 Å were collected at the F1 station at CHESS. The diffraction patterns were viewed and indexed using the programs *XDISPLAYF* and *DENZO* (Otwinowski, 1993). The orientation matrix **A** obtained from *DENZO* was then input to the program *OSC* for image processing (Rossmann, 1979). The data set was scaled and postrefined using the *Purdue* package (Rossmann *et al.*, 1979). Rotation functions were calculated using the program *GLRF* (Tong & Rossmann, 1990, 1997). Patterson functions and data completeness were calculated using the *CCP*4 package (Collaborative Computational Project, Number 4, 1994).

3. Results and discussion

3.1. Crystals, data collection and processing

The crystallization and data collection have been described previously (Wikoff *et al.*, 1998). Data to about 5 Å were collected at the F1 station at CHESS using crystals grown directly in the capillaries, without draining (Wikoff *et al.*, 1998). The crystal was translated after each exposure. A total of 73 crystals were used. Depending on crystal size, most crystals produced between four and eight images. A few exceptionally large crystals produced up to 15 images. The images were indexed using the program *DENZO* (Otwinowski, 1993). A total of 416 images were collected in this experiment at CHESS. The crystal-to-detector distance was 680 mm, with an exposure time of 90 s and an oscillation angle of 0.3°. Unit-cell parameters were $a = 580$, $b = 625$, $c = 788$ Å, $\alpha = \beta = \gamma = 90.0°$ (Fig. 1).

During data processing, another crystal form was identified with a morphology indistinguishable from that of the monoclinic form. The unit-cell parameters determined using *DENZO* were $a = 579$, $b = 834$, $c = 1164$ Å, $\alpha = \beta = \gamma = 90.0°$. The volume is 5.62×10^8 Å^3, twice that of the monoclinic cell, indicating that there were probably four particles per cell. No further analysis of this cell was undertaken; fortunately, this crystal form does not occur frequently.

Images were processed using the *Purdue* image-processing suite (Rossmann, 1979; Rossmann *et al.*, 1979). The crystal orientation matrix (**A** matrix) obtained from *DENZO* was input to the processing program as the initial orientation. Each image contained approximately 2000 accepted whole reflections and 7000 accepted partial reflections, with an assumed mosaic spread of 0.1°. 256 of the images were incorporated into the final data set.

3.2. Space-group determination

To definitively assign the space group, it was necessary to carefully examine the agreement in the measured intensities between reflections across putative symmetry axes. Because the α, β and γ angles were 90.0°, it was important to ensure that a lower (monoclinic) symmetry was not incorrectly chosen. The *Purdue* image-processing program includes a subroutine which allows the user to assume different space groups and calculate an *R* factor for the symmetry-related reflections on an individual film ($R_{\rm sym}$). The axially aligned crystals had suggested that the 625 Å axis was the 2_1 axis. An image was identified which had 20 pairs of strong reflections related by twofold symmetry along this axis, with an $R_{\rm sym}$ of 5.3%. This confirmed that the 625 Å axis is a lattice twofold. All images used in the final data set which contain symmetry-related reflections on the same image had $R_{\rm sym}$ values between 3 and 9% when this monoclinic symmetry was assumed. Similar calculations assuming twofold symmetry along either the *a* axis or *c* axis produced $R_{\rm sym}$ values of 30–50%, indicating that these were not twofold axes. The crystal system is monoclinic.

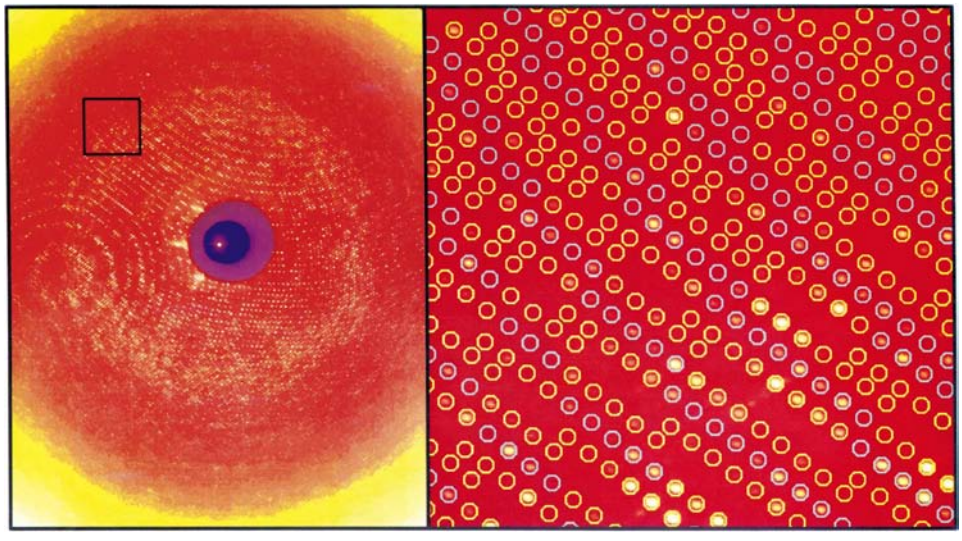

Figure 1
Left: a 0.3° oscillation photograph of an HK97 crystal recorded on an image plate at the CHESS F1 station. The outer resolution limit is 5 Å. Right: enlargement of the region in the square box of the pattern. The predicted pattern (circles) from *DENZO* indexing is overlayed with the observed pattern. The resolution at the center of the image is 8.5 Å and at the upper left corner 7.0 Å, the resolution to which the images were processed. The crystal-to-detector distance was 680 mm with $\lambda = 0.908$ Å.

In the monoclinic system, the *b* axis can be either a twofold (*P*2) or a twofold screw axis ($P2_1$). In space group *P*2, both particles must be in the *ac* plane, related by the twofold axis. This requires the distance between the particles to be 490 Å or less. The cryo-EM reconstruction shows that the minimum particle dimension is 550 Å along the threefold axes. It is not possible to pack two particles of these dimensions in a *P*2 cell without overlap and the space group must therefore be $P2_1$. Space group $P2_1$ requires systematic absences along the 0*k*0 lattice line when *k* is odd. There were many strong 0*k*0 reflections in the Head II data set

for k = even (Fig. 2). For k = odd, the reflections were either very weak (presumably incorrectly measured) or absent, confirming the presence of the screw axis along b. However, there is a possibility, which cannot entirely be ruled out, that the space group is actually triclinic, with a very strong pseudosymmetry about the b axis. In this case (and with the data scaled in the monoclinic system) however, the R_{sym} would presumably be higher (see below).

3.3. Data scaling and postrefinement

Although the space group is monoclinic, the lattice displays orthogonal axes within experimental error (β = 90.0°). This presents an 'orientation problem' in image indexing, allowing each crystal to be indexed with two possible orientations. The 90° β angle creates *mmm* symmetry in the positions of the reciprocal lattice points, but does not generate *mmm* symmetry in the reflection intensities. Therefore, it is not possible to determine the correct orientation from the lattice alone; the relative intensities must be examined for symmetry. The orientation can be determined by scaling the image processed with both orientations to a reference data set and comparing the individual R factors for that image. A typical image had an R_{scale} = 7.5% for the correct orientation and greater than 40% for the incorrect one. Thus, the correct orientation was obvious. Generating a consistent data set is a 'boot-strap' procedure in which all patterns must be referred to a reference data set. The initial data set was created by scaling together images from a single crystal, and a more extensive reference data set was generated by scaling additional images to that crystal, testing the orientation of each, for a total of 25 images.

There were 256 images included in the final data set. The post-refined cell dimensions were a = 579.9, b = 626.2, c = 788.1 Å, β = 90.0°. The overall completeness to 7 Å is 66% with 879441 reflections (Fig. 3). The overall R factor after post-refinement was 7.7% including all data which has $I/\sigma(I) > 2$.

Table 1
Peaks in the locked self-rotation function.

	φ	ψ	κ
Particle *A*	11.0	49.0	83.0
Particle *B*	8.4	48.2	84.2

3.4. Determination of the particle orientations

The rotation function (Rossmann & Blow, 1962) was used to determine the orientation of the two particles in the unit cell. A self-rotation function for κ = 72° (fivefold search) between 12 and 7 Å was calculated using the program *GLRF* (Tong & Rossmann, 1990; Fig. 4). Approximately 10% of the data were used as 'large terms' in the calculation and a radius of integration of 325 Å was employed. The stereographic plot indicated that the peak positions were consistent with an icosahedral set of symmetry elements. Each peak was split, indicating that the two particles were in similar, but not identical, orientations. An icosahedral twofold axis was close to, but not precisely parallel to, the crystallographic b axis (2_1 screw). An orthogonal icosahedral twofold axis was rotated approximately 18° away from the a axis. Self-rotation functions for κ = 120° (threefold) and κ = 180° (twofold) were also calculated and the results confirmed those from the fivefold search.

A locked self-rotation function (Tong & Rossmann, 1990), which considers all 60 icosahedral symmetry operators simultaneously, was calculated in order to determine the orientation with greater accuracy (Fig. 5). The calculation was performed between 12 and 7 Å and produced two peaks, one for each particle (Table 1). These peaks are related by crystallographic symmetry.

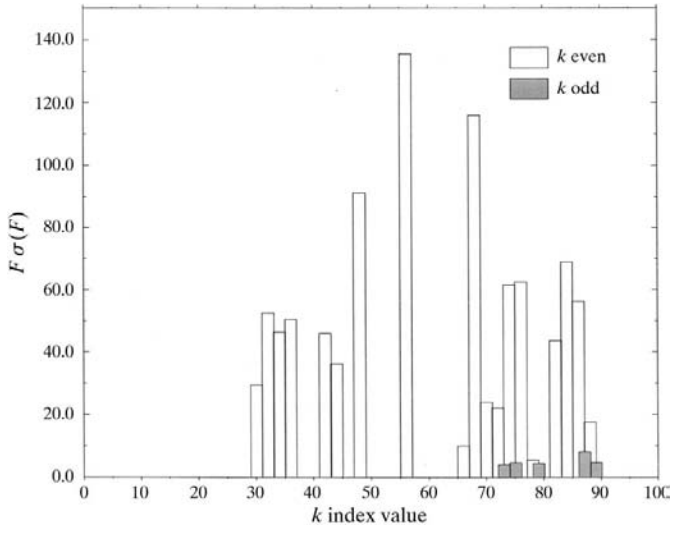

Figure 2
Plot of $|F_{obs}|/\sigma(|F_{obs}|)$ *versus* the Miller index k for the $0k0$ lattice line in the final merged data set. Values for even reflections are unfilled and values for odd reflections measured above background are shaded.

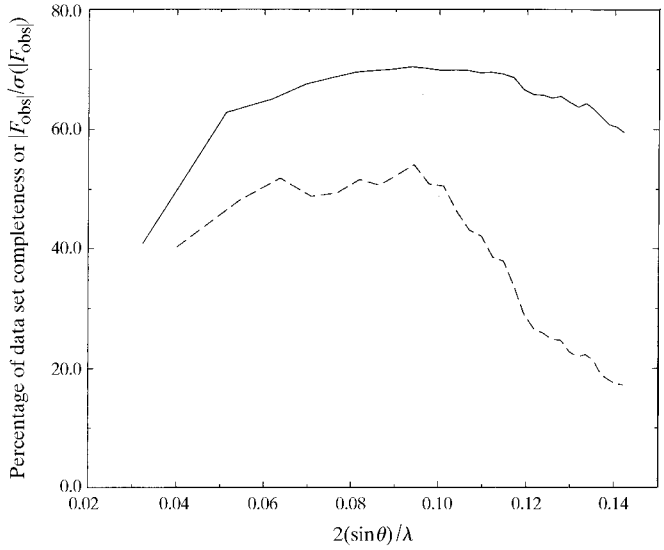

Figure 3
Data completeness (solid line) and $|F_{obs}|/\sigma(|F_{obs}|)$ (dashed line) plotted *versus* resolution.

A graphical representation of the constellation of symmetry elements consistent with these solutions is shown in Fig. 6. The position of these two locked rotation-function peaks agreed with the results of the self-rotation function. Each self-rotation function (κ = 72, 120, 180°) produced a set of peaks that was consistent with the locked rotation function. The agreement in the orientation and degree of peak splitting with the κ = 72° map (compare Figs. 4 and 6) was particularly striking.

3.5. Determination of the particle packing and positions

The particle volume, using a sphere with radius 275 Å (based upon on the dimension along the threefold axis in the cryo-EM reconstruction), is 8.711×10^7 Å^3. Table 2 shows the volume occupied in the unit cell by solid spheres and the V_m calculations. This indicates that the most reasonable packing is with two particles per cell. Each particle has a mass of 13.0×10^6 Da; with two particles per cell, the V_m for the empty particle is 11.0. This value is very high, owing to the fact that the particles contain no nucleic acid. When the calculation is performed assuming that the particles contained genomic dsDNA, the V_m is 3.7, a very reasonable value.

Table 2
Volume calculations.

Particles per cell	1	2	3
Cell volume occupied by sphere(s) (%)	30.4	60.8	91.3
V_m, empty capsid	21.9	11.0	7.3
V_m, full capsid	7.3	3.7	1.8

It is necessary to determine accurately the particle positions for phase determination by molecular replacement. For two spheres placed in a $P2_1$ cell, the lowest energy packing arrangement places the particles at the positions A ($\frac{1}{4}, y, \frac{1}{4}$) and B ($\frac{3}{4}, y + \frac{1}{2}, \frac{3}{4}$), where y is arbitrary because the monoclinic space group is polar.

From the cryo-EM reconstruction it is known that the Head II particle has the shape of an icosahedron with flat faces

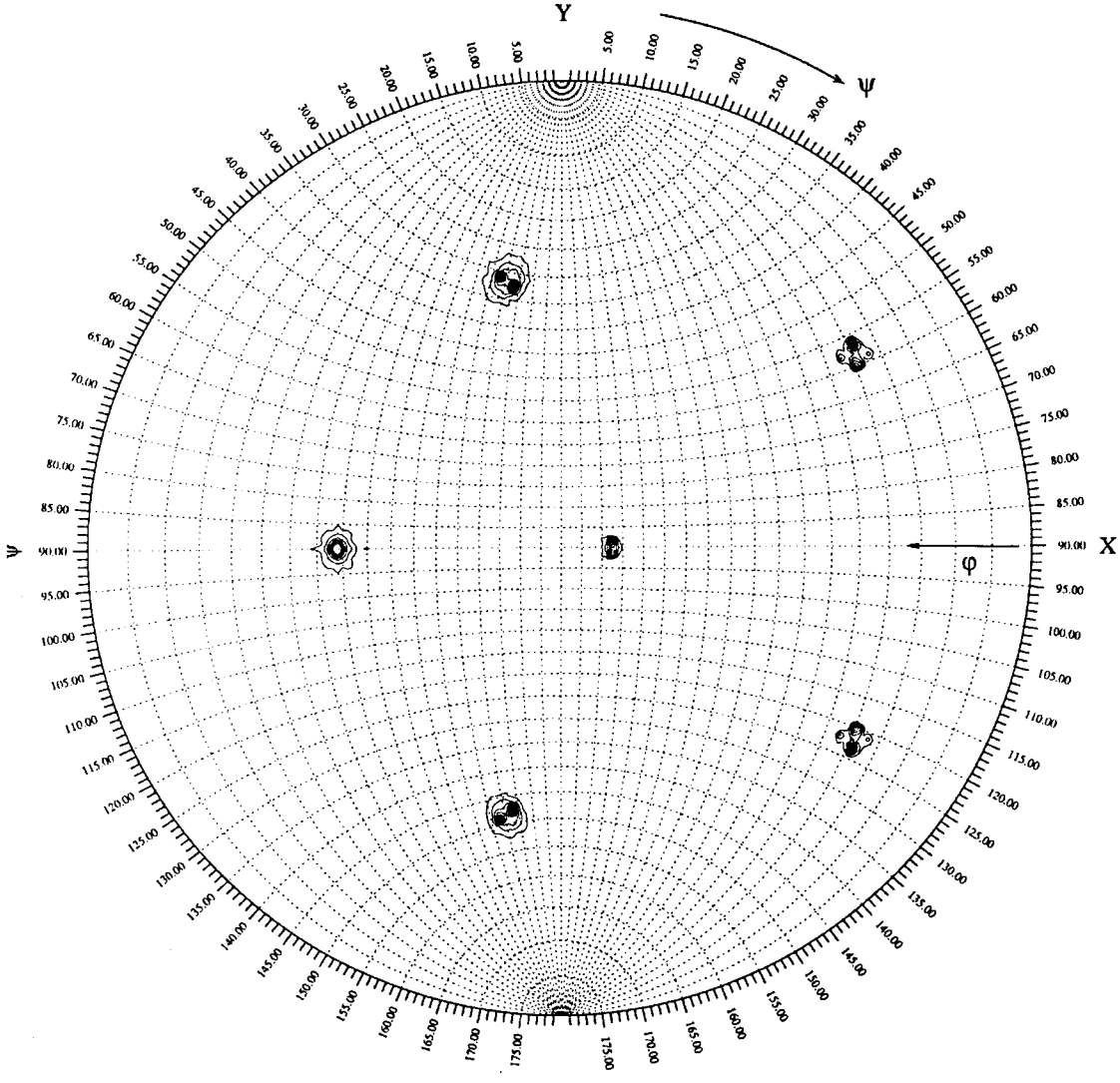

Figure 4
Self-rotation function calculated between 12 and 7 Å for κ = 72° (fivefold search). The rotation function indicates that an icosahedral twofold axis is almost parallel to the crystal *b* axis. The splitting of each peak is a consequence of the slight deviation from the parallel orientation.

roughly perpendicular to the icosahedral threefold axes (Conway *et al.*, 1995). Therefore, an icosahedron was chosen to model the particle packing. The size of the particle was determined by measuring along symmetry axes in images of the cryo-EM reconstruction (Conway *et al.*, 1995). The icosahedra in the orientation determined by the rotation function were placed in the unit cell using the display program *O* (Jones *et al.*, 1991). The distances between the particles were calculated with their centers at ($\frac{1}{4}$, 0, $\frac{1}{4}$) and ($\frac{3}{4}$, $\frac{1}{2}$, $\frac{3}{4}$). This packing analysis is summarized in Table 3 and illustrated in Fig. 7. The particle dimensions determined from the cryo-EM reconstruction are systematically shorter than the dimensions suggested by the crystal packing, indicating that the particles may be slightly larger at room temperature in the crystal. The particles must be close to their minimum energy (isotropic) packing arrangement, as movement by a significant distance (∼10 Å) away from this position results in particle overlap. The closest contact is along an icosahedral twofold axis nearly coincident with one set of the crystallographic body diagonals (1, 1, 1) and (−1, 1, −1). The particle twofold axes are also aligned in contact along the *b*-axis direction. The icosahedral threefold faces are in contact along the *a* axis and the other body diagonals (1, 1, −1) and (−1, 1, 1) directions. The flat threefold face of the particle visualized in the cryo-EM

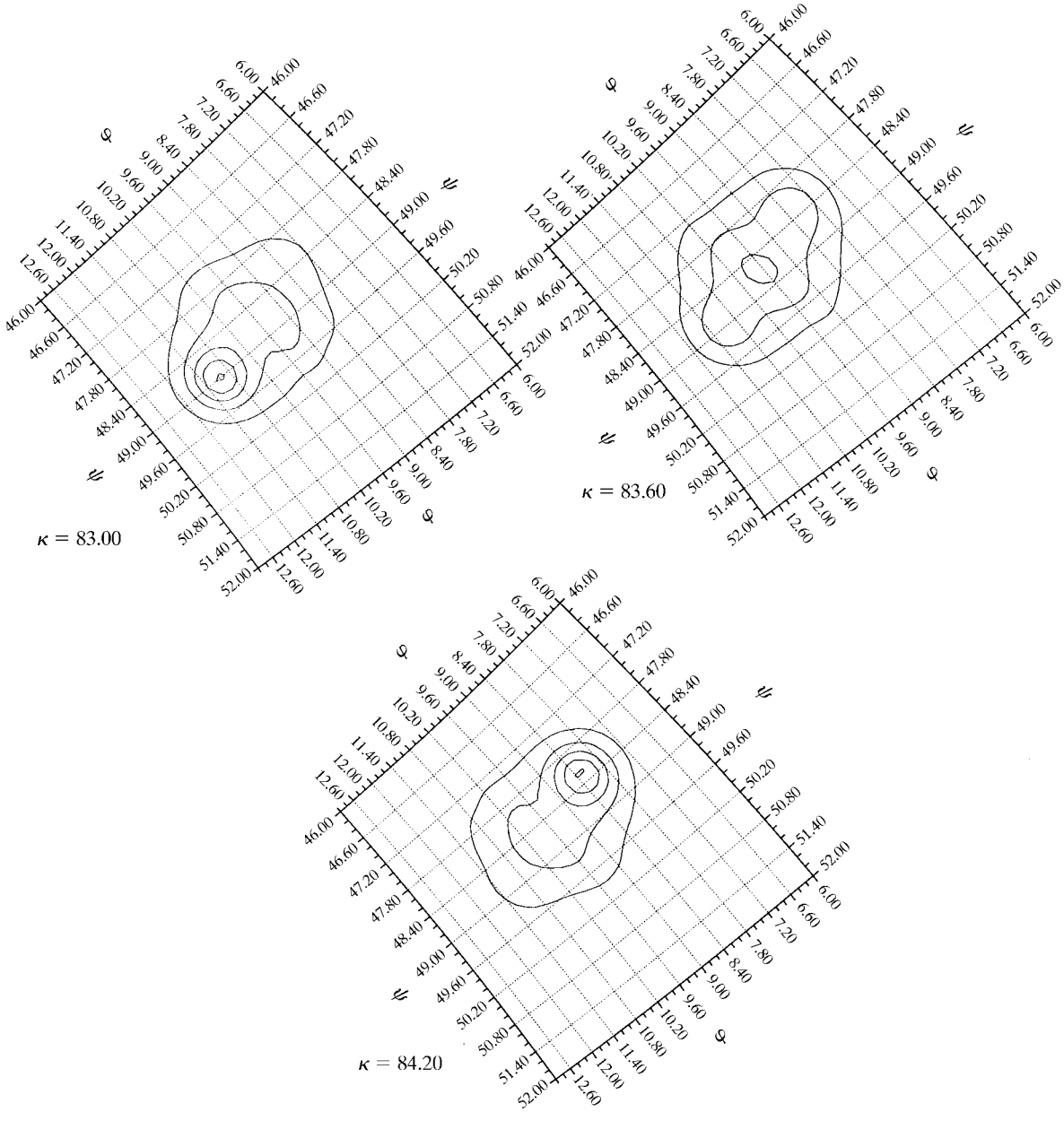

Figure 5
The locked self-rotation function between ψ = 46–52° and φ = 6–13°. The map was contoured from 2σ in steps of 1σ. Three sections are plotted, for κ = 83.0° (top left), 83.6° (top right) and 84.2° (bottom). The two highest peaks are at φ = 11.0, ψ = 49.0 and κ = 83.0° and at φ = 8.4, ψ = 48.2 and κ = 84.2°, corresponding to the two particles in the unit cell.

Table 3
$P2_1$ cell particle packing.

Axis or direction	Contact type	Cryo-EM dimension (Å)†	Standard icosahedron dimension (Å)‡	Particle packing distance (Å)§
a	Threefold	550	538	580
b (2_1)	None	—	—	625
c	None	—	—	790
Body diagonal (1, 1, 1) (−1, 1, −1)	∼ Twofold	>570	576	576
Body diagonal (1, 1, −1) (−1, 1, 1)	∼ Threefold	550	538	576

† Dimensions of the cryo-EM reconstruction along the icosahedral axis in column 2. ‡ Dimension of an icosahedron along the icosahedral axis in column 2, assuming that the dimension along the icosahedral twofold axis is 576 Å. § Distance along the unit-cell axis or direction divided by the number of particles packed along that direction.

reconstruction (Conway *et al.*, 1995) should provide a larger contact surface area than the twofold axis edge. The approximately 19° rotation of the particle about the *b* axis allows these relatively flat icosahedral threefold faces to pack along the *a* axis and two body-diagonal directions. Packing these threefold faces parallel requires the β angle to be 90.0°. If the β angle deviated statistically from 90°, these faces would not be parallel.

The packing analysis was independently confirmed by calculation of the Harker section of the Patterson map. In space group $P2_1$, the screw axis along β results in a Harker section at $v = \frac{1}{2}$ in the Patterson map. If the particles were close to $(\frac{1}{4}, y, \frac{1}{4})$ and $(\frac{3}{4}, \frac{1}{2} + y, \frac{3}{4})$ and if, as indicated by the rotation function, the particles were in similar orientations, there should be a Harker peak at $u = \frac{1}{2}$, $w = \frac{1}{2}$. A Patterson map at $v = \frac{1}{2}$ was calculated between 40 and 20 Å using the *CCP*4

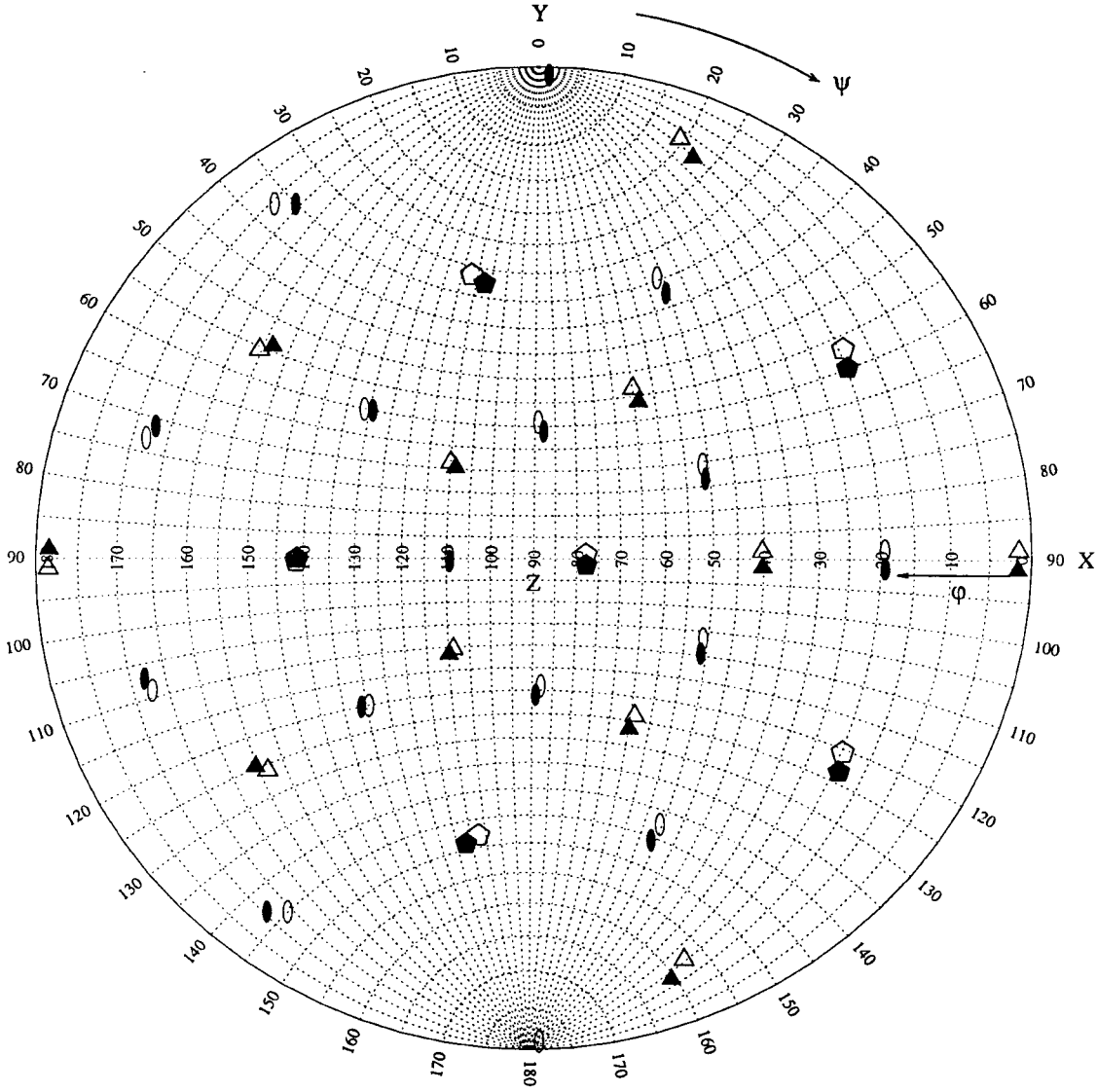

Figure 6
Particle orientations as determined by the locked self-rotation function, calculated between 12 and 7 Å. The peak positions are identical to those calculated by the self-rotation function. Note particularly the agreement in the orientation and degree of peak splitting with the $\kappa = 72°$ map (Fig. 4).

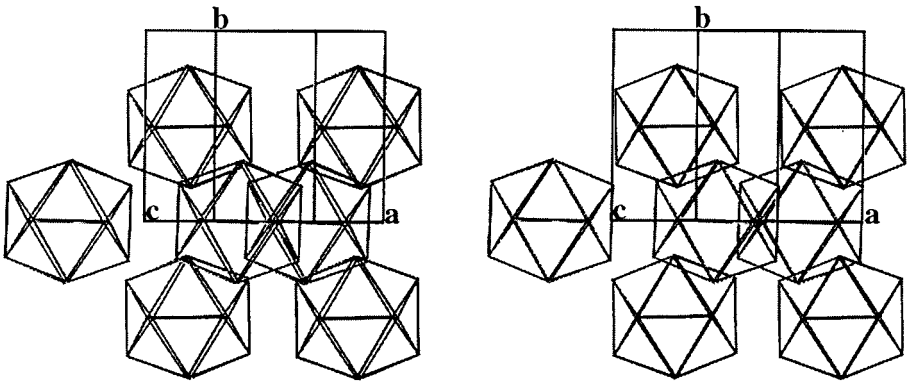

Figure 7
Packing diagram illustrating the arrangement of particles in the $P2_1$ unit cell. An icosahedral twofold axis is nearly aligned with the crystallographic *b* axis and a particle threefold axis is closely aligned with the *a* axis. The unit cell was rotated 18° about the *b* axis so that an icosahedral twofold axis is perpendicular to the plane of the paper. The diameter of the particles has been reduced to 400 Å for clarity.

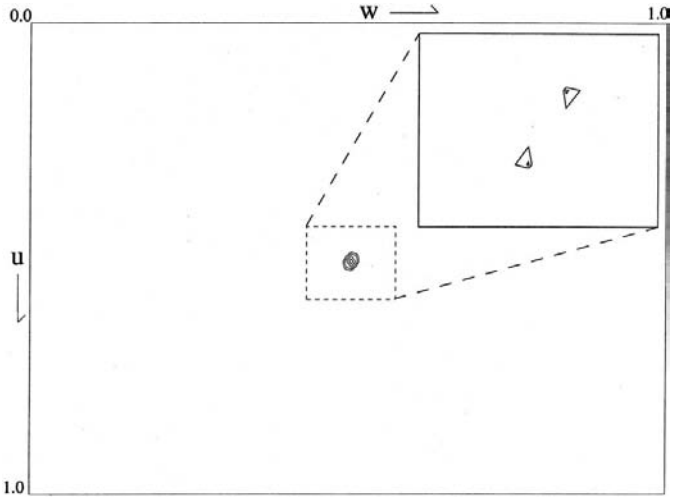

Figure 8
The Harker section of the Patterson map ($v = \frac{1}{2}$), calculated in the 40.0–20.0 Å resolution range. The map was contoured from 10σ in steps of 5σ. The horizontal axis is along *w* and the vertical axis is along *u*. There is a single peak at $u = \frac{1}{2}$, $w = \frac{1}{2}$. This confirms the rotation-function result that an icosahedral twofold axis is close to parallel to the *b* axis. It also indicates that the particle positions are close to the ideal packing arrangement of $(\frac{1}{4}, y, \frac{1}{4})$ and $(\frac{3}{4}, y + \frac{1}{2}, \frac{3}{4})$. Inset: at 23–15 Å resolution the peak is split because of the deviation of the icosahedral twofold from the *b* axis.

package (Collaborative Computational Project, Number 4, 1994) (Fig. 8). There was a single peak at the expected position. When the Harker section was calculated at higher resolution (23–15 Å) the peak was split. The splitting was caused by the slight deviation of the icosahedral twofold away from being parallel to the *b* axis. The results of the Patterson function confirmed the particle orientation and the expected packing arrangement. A similar effect in the Harker section was seen in the structure determination of canine parvovirus (Tsao *et al.*, 1992). The space group is also $P2_1$ with particles in close, but not exactly aligned, orientations. A single peak in the Harker section at low resolution becomes split and diminished in magnitude at higher resolution.

3.6. Summary

In this paper we have described the data processing, scaling and post-refinement of the Head II data set. The space group has been definitively determined to be monoclinic ($P2_1$). The particle orientation has been determined by the rotation function, its position established by examination of the Patterson function and the packing of the particles into the unit cell has been characterized. Thus, all the crystallographic parameters for molecular replacement have been determined. Phase determination will be initiated with molecular-replacement real-space averaging using the cryo-EM map of Head II empty capsids (Conway *et al.*, 1995)

We are grateful to the staff at CHESS for assistance with data collection and to CHESS for the award of synchrotron time (proposal 705) on beamline F1 for this project. This is manuscript number 11340-MB from the Scripps Research Institute. This work was supported by NIH grants AI40101 to JEJ and GM47795 to RWH.

References

Casjens, S. & Hendrix, R. (1988). *The Bacteriophages*, edited by R. Calendar, pp. 15–91. New York: Plenum.
Collaborative Computational Project, Number 4 (1994). *Acta Cryst.* D**50**, 760–763.
Conway, J. F., Duda, R. L., Cheng, N., Hendrix, R. W. & Steven, A. C. (1995). *J. Mol. Biol.* **253**(1), 86–99.
Dokland, T., Lindqvist, B. H. & Fuller, S. D. (1992). *EMBO J.* **11**(3), 839–846.
Dokland, T. & Murialdo, H. (1993). *J. Mol. Biol.* **233**(4), 682–694.
Jones, T. A., Cowan, S., Zou, J. Y. & Kjeldgaard, M. (1991). *Acta Cryst.* A**47**, 110–119.
King, J., Botstein, D., Casjens, S., Earnshaw, W., Harrison, S. & Lenk, E. (1976). *Philos. Trans. R. Soc. London Ser. B*, **276**(943), 37–49.
Li, Y., Thomas, G. J. Jr, Fuller, M. & King, J. (1981). *Prog. Clin. Biol. Res.* **64**, 271–283.
Liddington, R. C., Moulai, Y. Y., Sahli, R., Benjamin, T. L. & Harrison, S. C. (1991). *Nature (London)*, **354**, 278–284.
Murphy, F. A., Fauquet, C. M., Bishop, D. H. L., Ghabrial, S. A., Jarvis, A. W., Martelli, G. P., Mayo, M. A. & Summers, M. D. (1995). Editors. *Virus Taxonomy: Classification and Nomenclature of Viruses.* New York: Springer–Verlag.
Newcomb, W. W., Homa, F. L., Thomsen, D. R., Booy, F. P., Trus, B. L., Steven, A. C., Spencer, J. V. & Brown, J. C. (1996). *J. Mol. Biol.* **263**, 432–446.
Otwinowski, Z. (1993). *Proceedings of the CCP4 Study Weekend. Data Collection and Processing*, edited by L. Sawyer, N. Isaacs & S. Bailey, pp. 56–62. Warrington: Daresbury Laboratory.

Prasad, B. V., Prevelige, P. E., Marietta, E., Chen, R. O., Thomas, D., King, J. & Chiu, W. (1993). *J. Mol. Biol.* **231**(1), 65–74.
Prevelige, P. E. Jr, Thomas, D., Aubrey, K. L., Towse, S. A. & Thomas, G. J. Jr (1993). *Biochemistry*, **32**(2), 537–543.
Roberts, M. M., White, J. L., Grütter, M. G. & Burnett, R. M. (1986). *Science*, **232**, 1148–1151.
Rossmann, M. G. (1979). *J. Appl. Cryst.* **12**, 225–238.
Rossmann, M. G. & Blow, D. M. (1962). *Acta Cryst.* **15**, 24–31.
Rossmann, M. G., Leslie, A. G. W., Abdel-Meguid, S. S. & Tsukihara, T. (1979). *J. Appl. Cryst.* **12**, 570–581.
Steven, A. C., Greenstone, H., Bauer, A. C. & Williams, R. W. (1990). *Biochemistry*, **29**(23), 5556–5561.
Stroud, R. M., Serwer, P. & Ross, M. J. (1981). *Biophys. J.* **36**(3), 743–757.
Thomas, G. J. Jr, Li, Y., Fuller, M. T. & King, J. (1982). *Biochemistry*, **21**(16), 3866–3878.
Tong, L. & Rossmann, M. G. (1997). *Methods Enzymol.* **276**, 594–611.
Tong, L. A. & Rossmann, M. G. (1990). *Acta Cryst.* A**46**(10), 783–792.
Tsao, J., Chapman, M. S., Wu, H., Agbandje, M., Keller, W. & Rossmann, M. G. (1992). *Acta Cryst.* B**48**(1), 75–88.
Trus, B. L., Booy, F. P., Newcomb, W. W., Brown, J. C., Homa, F. L., Thomsen, D. R. & Steven, A. C. (1996). *J. Mol. Biol.* **263**, 447–462.
Wikoff, W. R., Duda, R. L., Hendrix, R. W. & Johnson, J. E. (1998). *Virology*, **243**(1), 113–118.